A&A 531, A116 (2011)
DOI: 10.1051/0004-6361/201016338

Astronomy & Astrophysics

X-ray observations of highly obscured $\tau_{9.7\ \mu m} > 1$ sources: an efficient method for selecting Compton-thick AGN?

I. Georgantopoulos[1,2], K. M. Dasyra[3,4], E. Rovilos[5], A. Pope[6,7], Y. Wu[8], M. Dickinson[6], A. Comastri[1], R. Gilli[1], D. Elbaz[3], L. Armus[8], and A. Akylas[2]

[1] INAF-Osservatorio Astronomico di Bologna, via Ranzani 1, 40127 Bologna, Italy
e-mail: ioannis.georgantopoulos@oabo.inaf.it
[2] Institute of Astronomy & Astrophysics, National Observatory of Athens, Palaia Penteli, 15236 Athens, Greece
[3] Laboratoire AIM, CEA/DSM – CNRS – Université Paris Diderot, Irfu/Service d' Astrophysique, CEA Saclay, Orme des Merisiers, 91191 Gif-sur-Yvette Cedex, France
[4] Observatoire de Paris, LERMA (CNRS:UMR8112), 61 Av. de l' Observatoire, 75014 Paris, France
[5] Max Planck Institut für Extraterrestrische Physik, Giessenbachstraße, 85748 Garching, Germany
[6] National Optical Astronomy Observatory, 950 North Cherry Avenue, Tucson, AZ 85719, USA
[7] Department of Astronomy, University of Massachusets, Amherst, MA01003, USA
[8] Spitzer Science Center, California Institute of Technology, MS 220-6, Pasadena, CA 91125, USA

Received 16 December 2010 / Accepted 22 April 2011

ABSTRACT

Observations with the IRS spectrograph onboard *Spitzer* have found many sources with very deep Si features at 9.7 μm, that have optical depths of $\tau > 1$. Since it is believed that a few of these systems in the local Universe are associated with Compton-thick active galactic nuclei (hereafter AGN), we set out to investigate whether the presence of a strong Si absorption feature is a good indicator of a heavily obscured AGN. We compile X-ray spectroscopic observations available in the literature on the optically-thick ($\tau_{9.7\ \mu m} > 1$) sources from the 12 μm IRAS Seyfert sample. We find that the majority of the high-τ optically confirmed Seyferts (six out of nine) in the 12 μm sample are probably Compton-thick. Thus, we provide direct evidence of a connection between mid-IR optically-thick galaxies and Compton-thick AGN, with the success rate being close to 70% in the local Universe. This is at least comparable to, if not better than, other rates obtained with photometric information in the mid to far-IR, or even mid-IR to X-rays. However, this technique cannot provide complete Compton-thick AGN samples, i.e., there are many Compton-thick AGN that do not display significant Si absorption, with the most notable example being NGC 1068. After assessing the validity of the high 9.7 μm optical-depth technique in the local Universe, we attempt to construct a sample of candidate Compton-thick AGN at higher redshifts. We compile a sample of seven high-τ *Spitzer* sources in the Great Observatories Origins Deep Survey (GOODS) and five in the *Spitzer* First-Look Survey. All these have been selected to have no PAH features ($EW_{6.2\ \mu m} < 0.3\ \mu$m) to maximise the probability that they are bona-fide AGN. Six out of the seven GOODS sources have been detected in X-rays, while for the five FLS sources only X-ray flux upper limits are available. The high X-ray luminosities ($L_X > 10^{42}$ erg s^{-1}) of the detected GOODS sources corroborates that these are AGN. For FLS, ancillary optical spectroscopy reveals hidden nuclei in two more sources. SED fitting can support the presence of an AGN in the vast majority of sources. Owing to the limited photon statistics, we cannot derive useful constraints from X-ray spectroscopy on whether these sources are Compton-thick. However, the low $L_X/L_{6\ \mu m}$ luminosity ratios, suggest that at least four out of the six detected sources in GOODS may be associated with Compton-thick AGN.

Key words. X-rays: general – X-rays: diffuse background – X-rays: galaxies – infrared: galaxies

1. Introduction

Hard X-rays (2−10 keV) are extremely efficient in detecting AGN, as they can penetrate large columns of dust and gas. This allowed the *Chandra* and *XMM-Newton* missions to map the AGN universe with unprecedented detail. In particular, about 90% of the X-ray background has been resolved (Alexander et al. 2003; Luo et al. 2008), revealing a sky density in the CDF-N of >5000 deg^2 (Bauer et al. 2004). The majority of these sources are obscured AGN, presenting column densities $>10^{22}$ cm^{-2} (e.g. Tozzi et al. 2006; Akylas et al. 2006).

However, even the hard X-ray surveys may be missing a substantial fraction of the most heavily obscured sources, the Compton-thick AGN, which have column densities $>10^{24}$ cm^{-2}. Although this population remains elusive (see Comastri 2004 for a review), there is concrete evidence for its presence. The peak of the X-ray background at 20−30 keV (e.g. Frontera et al. 2007; Churazov et al. 2007; Moretti et al. 2009) can be reproduced only by invoking a significant number of Compton-thick sources at moderate redshifts. However, the exact density of Compton-thick sources required by X-ray background synthesis models still remains an open issue (Gilli et al. 2007; Sazonov et al. 2008; Treister et al. 2009a). Additional evidence of a numerous Compton-thick population comes from the directly measured space density of black holes in the local Universe (see Soltan 1982). It is found that the black hole space density is a factor of 1.5−2 higher than that predicted from the X-ray luminosity function (Marconi et al. 2004; Merloni & Heinz 2008). The exact number depends on the assumed efficiency of the conversion of gravitational energy to radiation. Direct searches in

the ultra-hard 20−70 keV band by Swift and INTEGRAL did not detect large numbers of Compton-thick sources (e.g. Ajello et al. 2008; Tueller et al. 2008; Paltani et al. 2008; Winter et al. 2009). Nevertheless, it is possible that even these ultra-hard surveys are biased against the most heavily obscured reflection-dominated Compton-thick sources (Burlon et al. 2011). Owing to the limited imaging capabilities of these missions, the flux limit probed is very bright ($\sim 10^{-11}$ erg cm^{-2} s^{-1}) allowing only the detection of AGN in the local universe. At higher redshifts, some Compton-thick AGN have been reported in the deepest *XMM-Newton* and *Chandra* observations in the *Chandra* deep fields (Tozzi et al. 2006; Georgantopoulos et al. 2009; Comastri et al. 2011; Feruglio et al. 2011).

Mid-IR wavelength observations have attracted much attention because they provide an alternative way of detecting heavily obscured systems. This is because the absorbed radiation by circumnuclear dust is re-emitted in the IR part of the spectrum. Martínez-Sansigre et al. (2005) argue that a population of bright 24 μm AGN with no 3.6 μm detections is as numerous as unobscured QSOs at high redshift ($z > 2$). On the basis of X-ray stacking analysis, Daddi et al. (2007); Fiore et al. (2008); Georgantopoulos et al. (2008); Treister et al. (2009b); Eckart et al. (2010); Donley et al. (2010) propose that a fraction of infrared excess, 24 μm-bright sources are associated with Compton-thick AGN. These sources are found at high redshift ($z \sim 2$), and their contribution to the X-ray background is expected to be small (<1%; Treister et al. 2009a). In contrast, the bulk of the contribution to the X-ray background is produced at redshifts $z \sim 0.7-1$ (Gilli et al. 2007).

At high redshifts, mid-IR spectroscopy with *Spitzer*-IRS, has detected a number of sources with large columns of obscuring material, as inferred from their 9.7 μm Si features ($\tau > 1$; hereafter called high-τ sources; Dasyra et al. 2009). These systems could be associated with Compton-thick AGN. A local analog system is the nearby ULIRG NGC 6240 (Armus et al. 2006), which is well known in X-ray wavelengths to host a Compton-thick AGN (Vignati et al. 1999). There is little information available at X-ray wavelengths for these high-τ systems at higher redshift (Bauer et al. 2010).

The primary goal of this paper is to investigate whether an efficient way to identify Compton-thick AGN is indeed to look for sources with deep silicate absorption at 9.7 μm. The structure of the paper is as follows: we first compile a local sample of high optical-depth ($\tau_{9.7\,\mu m} > 1$) sources from the Wu et al. (2009) flux-limited *Spitzer*-IRS observations of the 12 μm Seyfert sample of Rush et al. (1993). We investigate the X-ray spectra available in the literature, to deduce how many of these high-τ objects are heavily obscured or Compton-thick. Finally, we compile a sample of high-τ AGN at higher redshift with available X-ray observations, using the *Chandra* Deep Fields, as well as the *Spitzer* FLS sample. Although these sources are faint in X-ray wavelengths (and thus it is difficult to derive with great certainty their X-ray spectral properties), we attempt to estimate whether they are heavily absorbed from their $L_x/L_{6\,\mu m}$ luminosity ratio.

We adopt $H_o = 70$ km s^{-1} Mpc^{-1}, $\Omega_M = 0.3$, and $\Omega_\Lambda = 0.7$ throughout the paper.

2. Sample selection

2.1. The local sample

We employ a sample of local galaxies with a deep Si absorption feature in the mid-IR, that are known to definitely host an AGN and also have X-ray data, so that the fraction of Compton-thick AGN among them can be quantified. An ideal data set for this purpose is the *Spitzer* IRS spectroscopic sample of Wu et al. (2009). These authors present low-resolution *Spitzer* 5.5−35 μm spectra for 103 galaxies from the 12 μm Seyfert sample (Rush et al. 1993). This is a complete, unbiased, flux-limited sample of local Seyfert galaxies, selected from the IRAS Faint Source Catalog by means of optical spectroscopy.

To identify sources with high optical depth at 9.7 μm ($\tau_{9.7}$) due to Si absorption, we use the 6 and 13 μm continuum flux to interpolate the intrinsic AGN unobscured flux at 9.7 μm in a similar way to Spoon et al. (2007). We subsequently measure $\tau_{9.7}$ by calculating the natural logarithm of its observed to intrinsic value. For screen extinction, this corresponds to $-\tau_{9.7}$. For sources without spectral coverage at 13 μm, we use the 6 and 7 μm continuum values to extrapolate at 9.7 μm. We reject all sources with optical depths smaller than one. Nonetheless, various spectral fitting techniques can lead to different $\tau_{9.7}$ values due to different continuum assumptions, see e.g. the small differences in our measurements of $\tau_{9.7}$ and those derived by Bauer et al. (2010) in the FLS sources. For this reason, we also run PAHFIT (see Smith et al. 2007) for all sources for which it is possible, using the parameters presented in Dasyra et al. (2009). We confirm that all of the sources selected with our primary technique also have $\tau_{9.7} > 1$ based on PAHFIT. The above re-analysis of the Wu et al. (2009) *Spitzer* spectra shows that $\tau_{9.7} > 1$ for eleven AGN (see Table 1). The IRS spectra of many of these sources were also discussed in Armus et al. (2007).

2.2. High-τ 9.7 μm AGN at higher redshift

To identify sources in the distant Universe that are deeply obscured in the mid-IR, we used all the *Spitzer*-IRS spectra available for the 4 deg^2 field of the First Look Survey (FLS), as well as for the CDF-N and CDF-S (~900 arcmin^2 in total) of the Great Observatories Origins Deep Survey (GOODS). The two surveys are complementary in targeting sources for our analysis. The FLS is a shallow 24 μm survey, whose spectra were limited to a depth of 0.9 mJy (Yan et al. 2007; Sajina et al. 2007; Dasyra et al. 2009), targeting luminous high-z galaxies. This is ideal for identifying many high-τ systems, as the highest amounts of obscuration are found in the sources with the highest infrared luminosity (Imanishi et al. 2010). However, the GOODS area has the most sensitive mid-IR and X-ray observations available. We select again sources with $\tau_{9.7\,\mu m} > 1$, using the methodology described above.

Since the initial sample selection is made at infrared wavelengths, we expect to find a significant number of non-AGN sources, which owe their infrared emission to dust heated by star-formation processes. To minimize the contamination by pure star-forming systems, we exclude sources with significant PAH emission at 6.2 or 11.3 or μm (see Fig. 1), since it has been demonstrated that AGN lack strong PAH features (e.g. Genzel et al. 1998; Hernán-Caballero et al. 2009). We define as PAH-poor sources (mostly AGN dominated) those that have $EW(6.2\,\mu m) < 0.3\,\mu m$, or $EW(11.3\,\mu m) < 0.3\,\mu m$ where the 6.2 Å wavelength is not covered.

There are 220 sources with IRS spectroscopy in the FLS sample, and we end up with 20 high-τ AGN in FLS using the method described above. Among these, there are six sources with *Chandra* observations available. Five of them have no obvious PAH features (see Fig. 1 and Table 3), while one (FLS-283) has $EW(11.3\,\mu m) = 0.68\,\mu m$ and is therefore not included in our sample. Pope et al. (in prep.) have consistently reduced and

Table 1. *Spitzer* IRS properties of the high-τ 9.7 μm AGN in the 12 μm sample.

Name	z	Type	τ	$\log[\nu L_{6\,\mu m}]$	AGN	$EW(6.2)$
(1)	(2)	(3)	(4)	(5)	(6)	(7)
Mrk 938	0.020	Sy2	1.2	10.09	0	0.440
NGC 1125	0.011	Sy2	1.0	9.12	0.81	0.258
I 08572+3915	0.058	Sy2	3.5	11.51	0.98	<0.021
UGC 5101	0.039	Sy1	1.4	10.52	0	0.229
NGC 3079	0.004	Sy2	1.3	9.10	0	0.458
Mrk 266	0.028	Sy2	1.0	10.03	0	0.608
Mrk 273	0.038	Sy2	1.7	10.51	0	0.192
Arp 220	0.018	Sy2	2.4	9.86	0	0.344
I 19254-7245	0.062	Sy2	1.2	11.03	0.88	0.064
NGC 7172	0.009	Sy2	1.9	9.75	0.2	0.045
NGC 7582	0.005	Sy2	1.0	9.56	0	0.274

Notes. The columns are: (1) Name; (2) Redshift; (3) Optical AGN type; (4) Optical depth at 9.7 μm; (5) Logarithm of νL_ν IR monochromatic luminosity; at 6 μm in units of solar luminosity; (6) Fraction of AGN contribution at 6 μm according to the spectral decomposition based on broad-band mid-IR photometry available from NED (see Sect. 3.2.3 for details of the models used); (7) Equivalent-width of PAH 6.2 μm feature in units of μm taken from Wu et al. (2009).

Table 2. X-ray properties of the high-τ 9.7 μm AGN in the 12 μm sample.

Name	z	N_H	$\log[L_x]$	X-ray Ref.	Mission	Comment
(1)	(2)	(3)	(4)	(5)	(6)	(7)
Mrk 938	0.020	40	42.30	1, 16	*XMM*	–
NGC 1125	0.011	–	41.97	2	Swift	–
I 08572+3915	0.058	–	41.30	3	*Chandra*	–
UGC 5101	0.039	140	41.67	4, 6, 7, 8, 11, 16	*Chandra*/*XMM*	a
NGC 3079	0.004	200	40.25	5, 16	*XMM*	a
Mrk 266	0.028	>160	41.7	1, 6	*XMM*/*Chandra*	a
Mrk 273	0.038	40	42.40	10, 16	*Chandra*	–
Arp 220	0.018	>100	40.96	7, 12, 14	*XMM*	b,c
I 19254-7245	0.062	>100	42.57	7, 8, 13	*BeppoSAX*	a
NGC 7172	0.009	8	42.20	9	*BeppoSAX*	–
NGC 7582	0.005	160	42.00	9, 15, 17	*BeppoSAX*	a

Notes. The columns are: (1) Name. (2) Redshift. (3) X-ray column density in units of 10^{22} cm^{-2}. (4) Logarithm of the obscured X-ray luminosity in the 2−10 keV band in units of erg s^{-1}. (5) X-ray spectroscopy reference: 1) Guainazzi et al. (2005); 2) Cusumano et al. (2010); 3) Iwasawa et al. (2009); 4) Imanishi et al. (2003); 5) Akylas & Georgantopoulos (2009); 6) Brassington et al. (2007); 7) Iwasawa et al. (2005); 8) Braito et al. (2003); 9) Dadina (2008); 10) Iwasawa et al. (2011); 11) González-Martin et al. (2009); 12) Ptak et al. (2003); 13) Georgantopoulos et al. (2010); 14) Clements et al. (2002); 15) Bianchi et al. (2009); 16) Brightman & Nandra (2011). (6) X-ray mission. (7) X-ray criterion on which the source is classified as Compton-thick: a. detection of the absorption turnover b. high-equivalent width Fe$K\alpha$ line c. Flat spectrum (see text for details).

analyzed all publicly available IRS spectra in both GOODS-N and ECDFS fields. For this paper, we search through the 150 GOODS IRS spectra database to find AGN with high $\tau_{9.7}$, selecting 15 sources. Eight of these sources are excluded because they have prominent PAH features with EW larger than 0.3 μm (see Table 5). The properties of the 12 sources in the high-redshift sample (seven GOODS and five FLS sources) are given in Table 3, while their IRS spectra are shown in Fig. 1.

2.3. Comparison between the high and low redshift samples

It is important to highlight the differences between the selection at low and high redshift. In the former, all sources are bona-fide AGN according to optical spectroscopy. Many sources would be classified as composite AGN/star-forming systems, on the basis of the EW of the 6.2 μm PAH feature.

Since there is no optical spectroscopy available for many sources in the high redshift sample, the AGN classification is based on the absence of strong PAH features. As discussed in Sect. 4.3.2, our AGN selection criterion is shown to be effective for at least eight out of twelve sources based on their high X-ray luminosities, and optical spectra and most probably all sources based on the measured MIR excess in their SED fitting. Therefore, the local and the high-redshift samples have different relative contributions to the star-formation in the total IR energy budget. Four sources in our local sample (Mrk 938 NGC 3079, Mrk 266, Arp 220) would not satisfy the $EW(6.2\ \mu m) < 0.3\ \mu$m selection criterion imposed in the high redshift sample.

3. Analysis

3.1. The local sample

3.1.1. X-ray observations

X-ray photometric observations exist for all sources in the local AGN sample. For one source (NGC 1125) only Swift-BAT observations are available at very high energies (>15 keV; Cusumano et al. 2010), and no X-ray spectrum can be derived. For another source (IRAS 08572+3915) there are *Chandra* observations available (Iwasawa et al. 2009), but unfortunately they are not sensitive enough to allow the derivation of the X-ray column through X-ray spectroscopy. For the remaining nine sources, we compile the X-ray spectroscopic results available in the literature in Table 2.

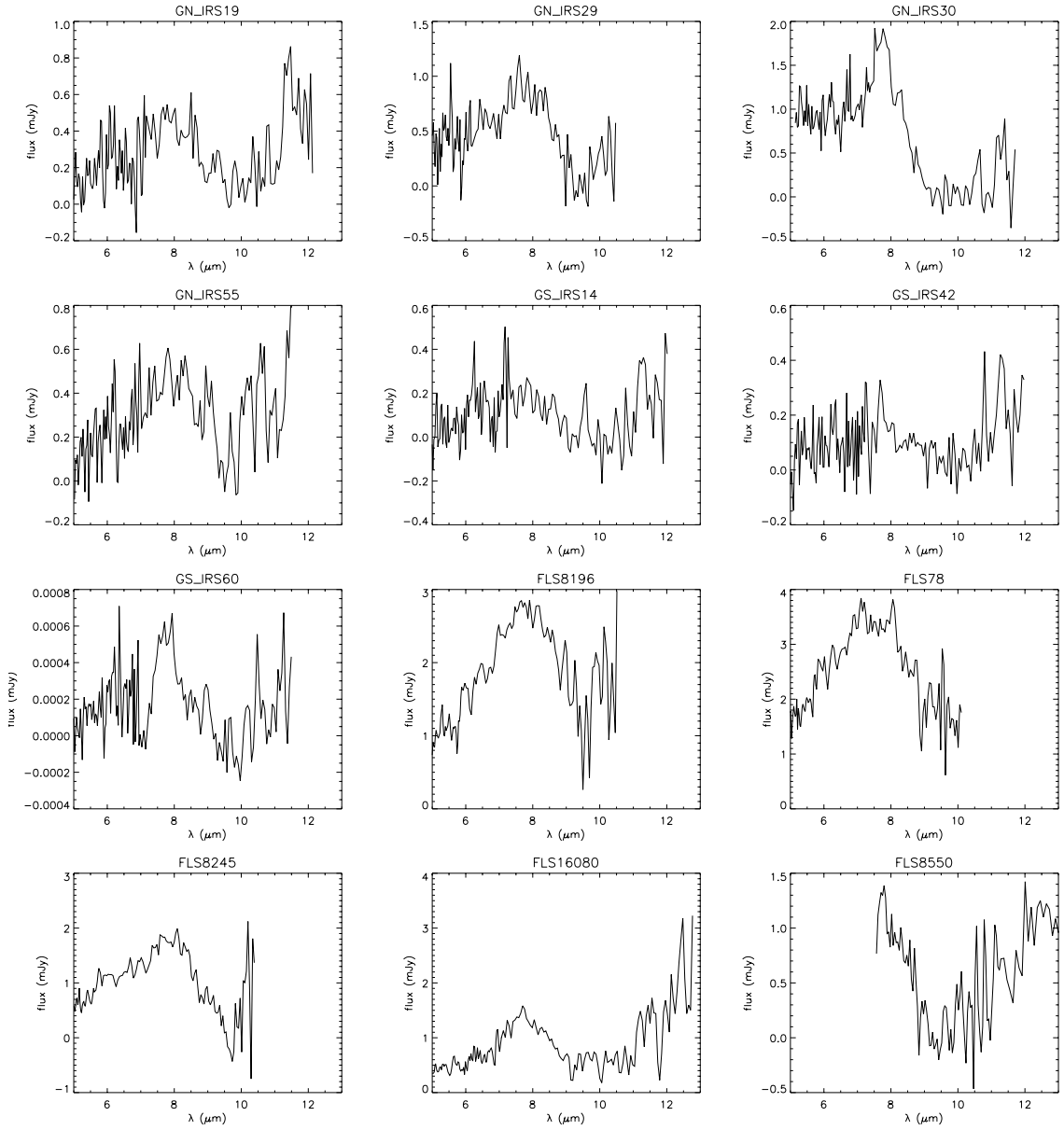

Fig. 1. IRS spectra of the GOODS and FLS sample.

3.1.2. X-ray spectra

The classification of a source as Compton-thick is based on one of the following criteria (see Georgantopoulos et al. 2009):

(a) The most reliable criterion is the detection of the absorption turnover at high energies. These are the transmission-dominated Compton-thick sources with relatively "mild" column densities of a couple of times 10^{24} cm^{-2}. In these sources, we can directly view the obscured component through the torus, even at energies below 10 keV (e.g. NGC 3079; Akylas & Georgantopoulos 2009).

(b) The detection of a high (~1 keV) equivalent-width (EW) Fe line.

(c) A "hard" spectrum with $\Gamma \sim 1$ or flatter. This is considered to be the signature of a reflection dominated Compton-thick source, where the X-ray emission comes solely from reflection from the backside of the torus (see e.g. Murphy & Yaqoob 2009).

Six of the nine sources for which X-ray spectra can be derived probably host a Compton-thick nucleus based on one of the above criteria (see Table 2). Out of these, UGC 5101 is probably the most debatable case: in a study of ULIRGs with large amounts of molecular gas, Georgantopoulos et al. (2010) detect a flat spectrum ($\Gamma \sim 1.2$) using *Chandra*, together with a high EW (~3.6 keV) FeKα line, in agreement with Ptak et al. (2003). The combination of a flat spectrum with a high EW FeKα line suggests a Compton-thick AGN. Imanishi et al. (2003) analyzed both the *XMM-Newton* and the *Chandra* data and found a considerably lower EW (~400 eV). González-Martin et al. (2009), using *Chandra*, claim the direct detection of a mildly Compton-thick AGN with a column density of $N_{\rm H} \approx 1.4 \pm 0.4 \times 10^{24}$ cm^{-2}. Finally, Brightman & Nandra (2011) report a column density of 10^{23} cm^{-2} by re-analyzing the available *XMM-Newton* data. We note that the same authors report a much lower column density (2×10^{23} cm^{-2}) for Mrk266 (NGC 5256) than the one derived by Guainazzi et al. (2005). NGC 7582 is one of the few known "changing-look" AGN, i.e. sources with past X-ray

Table 3. High-τ 9.7 μm AGN at higher redshift

Name	α	δ	z	S_8	τ	PAH EW	log[L_6]	log[L_{IR}]	AGN	Comment	AGN
(1)	(2)	(3)	(4)	(5)	(6)	(7)	(8)	(9)	(10)	(11)	(12)
CDF-N											
GN_IRS-19	12:35:55.1	+62:09:01	1.875[1]	0.097	2.43	<0.18	11.37	12.62	0.75	a, b, d, e	Y
GN_IRS-29	12:36:56.5	+62:19:37	2.2[2]	0.048	2.54	<0.11	11.83	12.62[1]	0.91	a, d, e	Y
GN_IRS-30	12:37:26.5	+62:20:26	1.76[2]	0.175	3.6	<0.07	11.92	12.74[1]	0.96	a, d, e	Y
GN_IRS-55	12:36:46.7	+62:14:46	2.004[3]	0.027	1.8	<0.09	11.49	12.40	0.58	a, b, d, e	Y
CDF-S											
GS_IRS-14	03:32:14.5	–27:52:33	1.87[2]	0.026	2.22	<0.20	11.16	12.66[1]	0.67	d, e	p
GS_IRS-42	03:32:25.9	–27:47:51	1.88[2]	0.02	1.78	<0.28	10.99	12.25[1]	0.32	a, d	Y
GS_IRS-60	03:32:40.0	–27:47:55	2.0[2]	0.045	1.35	<0.17	11.78	13.25	0.57	a, d, e	Y
FLS											
FLS-8196	17:15:10.2	+60:09:54	2.59[2]	12.5	1.32	<0.05	12.50	13.40	0.74	d, e, f	Y
FLS-78	17:15:38.2	+59:25:40	2.65[2]	12.7	1.49	<0.04	12.71	13.51	1	d, e	p
FLS-8245	17:15:36.3	+59:36:14	2.70[2]	24.	2.13	<0.05	12.38	13.25	0.98	d, e	p
FLS-16080	17:18:44.8	+60:01:15	2.01[2]	71.	2.17	<0.08	11.76	12.85	0.71	c, d, e	Y
FLS-8550	17:18:14.6	+59:56:05	0.87[2]	255.	2.74	<0.27	11.10	12.09[1]	0.70	d, e	p

Notes. The columns are: (1) Name; (2), (3) Equatorial *Spitzer* coordinates; (4) Redshift: [(1)] Chapman et al. (2005); [(2)] IRS from Pope et al. (2008) or Murphy et al. (2009) in the case of GOODS, or Sajina et al. (2007) in the case of FLS...; [(3)] Barger et al. (2008); (5) 8 μm flux in units of μJy; (6) optical depth at 9.7 μm; (7) PAH equivalent-width at 6.2 μm in units of μm (except in the case of FLS-8550 where the 11.3 μm EW is quoted); (8) Logarithm of the νL_ν monochromatic luminosity at 6 μm in units of solar luminosity as derived by IRS spectroscopy; (9) Logarithm of the 8−1000 μm IR luminosity in units of solar luminosity as derived from the SED fitting; [(1)] No photometry at rest-frame wavelengths >30 μm which constrains the far-IR luminosity; (10) fraction of AGN contribution at 6 μm according to the spectral decomposition; (11) evidence for the presence of an AGN: a) X-ray luminosity, b) radio-emission, c) broad optical line, d) absence (or weakness) of PAH feature, e) SED, f) broad-ish (>500 km s^{-1}) [OIII] line; (12) AGN classification: (Y) secure on the basis of the X-ray luminosity or optical spectroscopy, (p) probable on the basis of the mid-IR diagnostics i.e. low-EW PAHs and SED fitting.

observations in both a Compton-thin and a reflection-dominated state (Bianchi et al. 2009). The three high-τ AGN that are definitely not Compton-thick are Mrk 938, Mrk 273, and NGC 7172. These have column densities between $N_H = 8 \times 10^{22}$ cm^{-2} and 4×10^{23} cm^{-2}. For Mrk 273, Iwasawa et al. (2011) note that the X-ray emission may come from a different location than the IR nucleus. They also point out that the IR nucleus may be associated with a Compton-thick source, although the evidence for this remains weak.

3.2. Sources at high redshift

3.2.1. The X-ray observations

The FLS has few (and shallow; ~30 ks) X-ray data points, which are presented in Bauer et al. (2010). Their X-ray observations targeted primarily ULIRGs. There are X-ray observations available (all of them yielding upper limits) for only five out of the 20 high-τ AGN in FLS. However, the GOODS survey for the *Chandra* Deep Fields has the deepest X-ray images to date. The CDF-N was observed for 2 Ms (see Alexander et al. 2003). We examine the 2 Ms CDF-N X-ray images and find that all sources are detected in the total (0.3−8 keV) band. Three of the sources are in the catalog of Alexander et al. (2003), while the other one is marginally below the detection threshold of these authors. The CDF-S was originally observed for 2 Ms (Luo et al. 2008), while the field was observed for an additional 2 Ms. Here, we use the entire set of 4 Ms images. In the CDF-S, two sources (out of the three high-τ sources in this field) are detected in the total (0.3−8 keV) band.

3.2.2. X-ray spectra

Among the X-ray detections, we can derive low-quality X-ray spectra in five cases but in only three we can constrain both the photon-index and the hydrogen column density. We use XSPEC (Arnaud 1996) for the spectral fitting. We use the C-statistic (Cash 1979), leaving the data ungrouped. The errors correspond to the 90% confidence level. We fit a simple power-law with photoelectric absorption from cold material in all cases. First, leave both the photon index and column density as free parameters for the three sources with the highest quality photon statistics. The results are given in Table 4. There is no clear evidence of a Compton-thick source. GN_IRS-30 presents a very flat spectrum, with $\Gamma = 0.54$, but very large errors. To obtain more stringent constraints on the absorbing column density, we fix the photon-index to the commonly observed value of $\Gamma = 1.8$ (Dadina 2008). We see that the spectra of the sources GN_IRS-19 and GN_IRS-30 are heavily obscured with column densities ~10^{23} cm^{-2}.

3.2.3. Spectral energy distributions

To estimate the total infrared emission of the sources in the high redshift sample, and assess the possibility that they host an AGN, we fit their broad-band spectra with combinations of starburst and AGN templates. The starburst templates we use come from the SWIRE template library[1] (Polletta et al. 2007), which is a compilation of oberved SED of nearby galaxies, and from the sample of Chary & Elbaz (2001). The AGN templates we use come from Silva, Maiolino & Granato (2004), who combine nuclear SEDs of Seyferts with a range of absorption columns. We also construct a sample of AGN templates using the type-1 QSO SED from Richards et al. (2006) and applying dust absorption following Rosenthal et al. (2000), to account for the 9.7 μm absorption feature.

[1] www.iasf-milano.inaf.it/~polletta/templates/swire_templates.html

Table 4. X-ray properties of the high-redshift sample.

		Γ, N_H free		$\Gamma = 1.8$
Name	L_X	Γ	N_H	N_H
(1)	(2)	(3)	(4)	(5)
CDF-N				
GN_IRS-19[a]	43.5	$1.44^{+0.47}_{-0.44}$	$12.1^{+6.9}_{-5.5}$	$16.8^{+4.0}_{-3.8}$
GN_IRS-29	42.3	–	–	< 7.9
GN_IRS-30[b]	43.1	$0.54^{+1.18}_{-0.49}$	<17.5	17.0^{+16}_{-10}
GN_IRS-55[c]	42.3	$2.15^{+2.6}_{-1.18}$	<5.8	<4
CDFS-S				
GS_IRS-14	<42.9	–	–	–
GS_IRS-42[d]	42.3	–	–	<1.3
GS_IRS-60	42.1	–	–	–
FLS				
8196	<43.8	–	–	–
78	<44.1	–	–	–
8245	<43.8	–	–	–
16080	<43.7	–	–	–
8550	<43.7	–	–	–

Notes. The columns are: (1) Name [(a)] , [(b)], [(c)] sources 44, 423, and 243 respectively in the catalogue of Alexander et al. (2003); [(d)] source 240 in Luo et al. (2008). (2) Logarithm of the X-ray luminosity (2−10 keV) (or 3σ upper limits) uncorrected for absorption in units erg s^{-1}. Luminosities have been estimated from the X-ray spectral fits. Where there is no spectral fit, we assume $\Gamma = 1.4$. (3) Photon index. (4) Rest-frame column density in units of 10^{22} cm^{-2}. (5) Rest-frame column density in units of 10^{22} cm^{-2}, where $\Gamma = 1.8$.

Table 5. High-τ 9.7 μm sources not included in our sample because of a high PAH *EW*.

Name	α	δ	z	τ	PAH *EW*	log[L_6]	log[L_X]
(1)	(2)	(3)	(4)	(5)	(6)	(7)	(8)
GN_IRS-4	12:36:53.4	+62:11:39	1.27[2]	1.12	0.67	11.40	41.8
GN_IRS-11	12:36:21.3	+62:17:08	1.992[1]	1.55	1.18	11.41	<42.8
GN_IRS-13	12:37:34.5	+62:17:23	0.64[2]	1.37	0.48	11.27	41.3
GN_IRS-14	12:36:22.5	+62:15:44	0.639[2]	3.00	0.63	10.39	41.4
GN_IRS-15	12:37:11.4	+62:13:31	1.99[2]	1.09	0.78	10.74	42.8
GN_IRS-16	12:36:37.0	+62:08:52	2.02[2]	3.97	0.57	11.27	42.1
GN_IRS-20	12:36:03.2	+62:11:10	0.64[2]	2.32	0.60	10.68	41.5
GN_IRS-21	12:36:18.3	+62:15:50	2.00[2]	1.96	0.66	11.19	42.4
FLS-283	17:14:58.3	+59:24:11	0.94[2]	1.12	0.68	11.46	<43.1

Notes. The columns are: (1) Name; (2), (3) Equatorial *Spitzer* coordinates; (4) Redshift: [(1)] Chapman et al. (2005); [(2)] IRS from Pope et al. (2008), Murphy et al. (2009) in the case of GOODS or Sajina et al. (2007) in the case of FLS; (5) optical depth at 9.7 μm. (6) PAH equivalent-width at 6.2 μm, in units of μm (except in the case of FLS-283 where the 11.3 μm *EW* is quoted); (7) Logarithm of the νL_ν monochromatic luminosity at 6 μm in units of solar luminosity as derived by IRS spectroscopy; (8) X-ray luminosity (uncorrected for obscuration) in the 2−10 keV band in units erg s^{-1}.

The photometry we use for the GOODS-N and GOODS-S sources comes from the IRAC (3.6, 4.5, 5.8, and 8.5 μm) public GOODS data release and the SIMPLE survey (*Spitzer* IRAC/MUSYC Public Legacy in ECDF-S; Damen et al. 2011) respectively. MIPS photometry at 24 and 70 μm, comes from the FIDEL survey (Far-Infrared Deep Extragalactic Legacy survey; see Magnelli et al. 2009) and the 850 μm photometry in the GOODS-N from Pope et al. (2005). The FLS sources have IRAC and MIPS (70 μm) photometric values published in Sajina et al. (2007), while their MIPS (24 μm) and 1.2 mm fluxes are published in Sajina et al. (2008). In the IRS wavelength range, we bin the data every five datapoints and average their flux values, which gives us 30 photometric data points per source.

We use a χ^2 minimisation method to select the optimum combination of a starburst and an AGN template to fit our data. The results can be seen in Fig. 2. We calculate the 8−1000 μm luminosity by integrating the best-fit SED; the results are listed in Table 3. We note that six of the GOODS-N sources have their infrared luminosities published in Murphy et al. (2009), where a similar procedure was used in their calculation. Our L_{IR} values agree within a factor of 2 with the L_{IR} values of Murphy et al. (2009). Most of the sources of Table 3 require both a star-forming and an AGN template to fit the photometric points. The spectral decomposition (Fig. 2) suggests that the bulk of the mid-IR emission is produced by the AGN component. The exception is GS_IRS-42. In the case of this source, an F-test gives only an 8% probability that the AGN component is needed.

3.2.4. L_X/L_6 ratio

For faint sources such as those in the CDFs, it is difficult to apply X-ray spectroscopy diagnostics owing to the limited photon statistics. Alternatively, the L_X to $L_{6\,\mu m}$ ratio could be used to identify any highly obscured, Compton-thick AGN. One of the most reliable proxies of the intrinsic power of an AGN is considered to be the mid-IR 6 μm luminosity (e.g. Lutz et al. 2004; Maiolino et al. 2007). This wavelength region can contain significant emission from the hot dust heated by the AGN, and thus

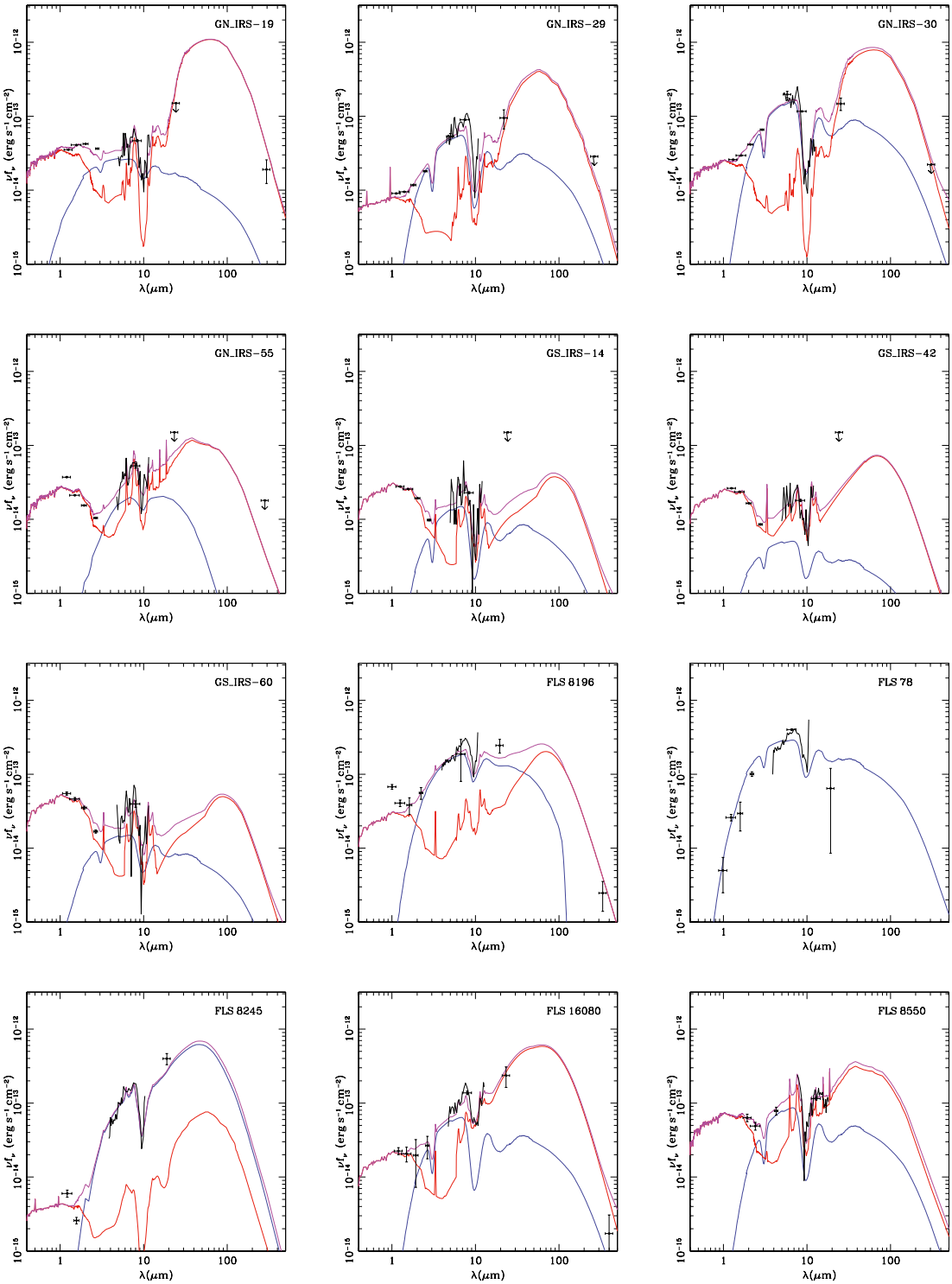

Fig. 2. Mid-IR rest-frame SEDs of the GOODS and FLS sample. The blue and red line denote the torus and star-forming contribution while the purple line denotes the sum of the two.

provides a reliable diagnostic of the AGN power. On the basis of this, Alexander et al. (2008) and Goulding et al. (2011) claim that very low X-ray to $L_{6\ \mu m}$ ratios, typically 30−40 times lower than those of unobscured AGN, is indicative of very strong attenuation at X-ray wavelengths and thus of Compton-thick sources.

We present the 2−10 keV luminosity, uncorrected for absorption, against the monochromatic 6 μm IR luminosity for both the 12 μm sample and the higher redshift sources in Fig. 3. We define very roughly a region where Compton-thick AGN reside, by scaling down the relation of Fiore et al. (2009) for the AGN in the COSMOS fields by 0.03. This is very roughly the amount of reflected emission in a type-2 AGN (Comastri 2004). Moreover, we show the scaled down L_X−$L_{6\ \mu m}$ relation, by the same amount, of AGN in the local Universe found by

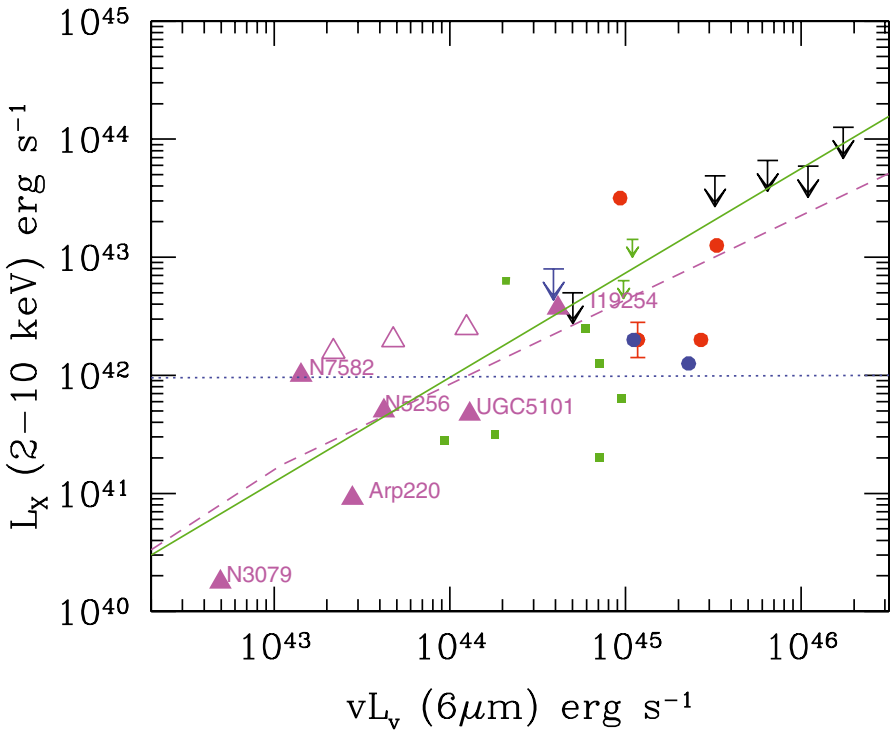

Fig. 3. Rest-frame (uncorrected for absorption) L_X versus $L_{6\,\mu m}$ luminosity diagram. The filled triangles correspond to the Compton-thick AGN in the 12 μm sample, while the open triangles correspond to the three heavily obscured but not Compton-thick AGN in the same sample. The red (blue) filled circles or upper limits denote the high-τ sources in the CDF-N (CDF-S). The black upper limits denote the FLS points. Finally, the green points (filled squares and small upper limits) denote the sources with considerable PAH emission that have not been included in our sample. The dash line (magenta) denotes the low $L_X/L_{6\,\mu m}$ area that should be populated by Compton-thick AGN. This line is derived from the average $L_X/L_{6\,\mu m}$ relation derived for the COSMOS AGN (Fiore et al. 2009) by scaling it down by a factor 0.03, which corresponds to the average flux of the reflection component in the 2−10 keV band relative to the intrinsic power-law component in local Compton-thick AGN (Comastri 2004). The solid line (green) corresponds to the luminosity-dependent Compton-thick line based on the Maiolino et al. (2007) relation, scaled down by the same amount. Finally, the horizontal dotted line at $L_X = 10^{42}$ erg s^{-1} denotes the upper limit to X-ray emission due to star-forming processes (Tzanavaris et al. 2006).

Lutz et al. (2004). Finally, we show the luminosity-dependent line predicted by Maiolino et al. (2007). The luminosity error bars do not play a major role relative to the uncertainties introduced by the use of different Compton-thick lines. We present a typical error-bar for one source. This includes both the photon statistics error as well as the uncertainty in the spectral model used for the conversion from flux to luminosity. Therefore, the uncertainties in this diagnostic are quite large.

Using as a guide our AGN in the local Universe for which we have reliable X-ray spectroscopy, we see that there is one Compton-thick source (NGC 7582) that lies above the local Compton-thick AGN regime. Moving to our AGN at higher redshift, there are four GOODS sources that could be classified as Compton-thick according to the $L_X/L_{6\,\mu m}$ diagnostic, i.e. GN_IRS-29, GN_IRS-55, GS_IRS-42, and GN_IRS-60. Taking into account only the X-ray detections, the fraction of possible Compton-thick sources would be 66% (4/6). The X-ray upper limits are all situated unconveniently above the Compton-thick regime. Under the extreme assumption that all upper limits are either associated or not with Compton-thick sources, the fraction of Compton-thick AGN could vary between 33% and 83%.

3.2.5. Contamination by star-forming galaxies.

Our selection criterion (low *EW* PAH) is chosen to minimise the number of star-forming galaxies (non-AGN) in our sample. The *EW* upper limits of our FLS sources are consistent with a high AGN contribution, close to 100% according to Fig. 5 of Sajina et al. (2007). The absence of strong PAH features is unlikely to be an artefact of low signal-to-noise ratio spectra. There is no trend for a dependence of the *EW* on the mid-IR flux (see Table 3). The two brightest FLS sources, with X-ray observations available, are among the sources with the lowest *EW*. Another possibility could be that the PAHs are possibly suppressed in star-forming galaxies with large amounts of absorption (e.g. Zakamska 2010). However, the region responsible for the silicate absorption is most probably located between the AGN torus and the narrow-line-region (e.g. Netzer et al. 2007). The most solid evidence that these silicates are mostly located close to the torus is that they are often seen in-emission in type-1 AGN and in absorption in type-2. In contrast, most of the PAH emission should originate from larger scales (Soifer et al. 2002). Furthermore, inspection of the strength of the 6.2 μm PAH feature of the rejected $\tau > 1$ sources in Table 5, shows that these display high PAH *EW* (up to $EW \sim 1.2$ μm) despite there being optically thick at 9.7 μm.

However, the most robust indicator of detection of an AGN can be provided by the level of its X-ray emission. Although a detection at X-ray wavelengths is generally sufficient to confirm the presence of an AGN, the GOODS fields probe extremely faint fluxes where a number of sources could be associated with normal galaxies (i.e. without an AGN) (Georgakakis et al. 2007; Ptak et al. 2007). These also have low $L_X/L_{6\,\mu m}$ ratios because their X-ray emission is intrinsically weak (instead of absorbed). We set the AGN detection limit to $L_X = 10^{42}$ erg s^{-1} as no local pure star-forming galaxy has ever presented a 2−10 keV luminosity above this threshold (see Tzanavaris et al. 2006). One of the most X-ray luminous star-forming galaxies is NGC 3256, which has a 2−10 keV luminosity of 2.5×10^{41} erg s^{-1}, but displays no evidence of AGN activity (Moran et al. 1999). Therefore, for all our six sources with X-ray detections, we can be confident that they are AGN, as they present X-ray luminosities above 10^{42} erg s^{-1}.

In agreement with the above classifications, two of our sources (GN_IRS-19 and GN_IRS-55) have additional evidence of an AGN via excess of radio emission (Del Moro et al., in prep.). FLS-8196 presents an [OIII] line with a *FWHM* of ≈800 km s^{-1} (Sajina et al. 2008), which is typical of emission from the AGN narrow-line-region (Zakamska et al. 2003). FLS-16080 displays a broad CIVλ1550 Å emission line, with

a *FWHM* of ≈2500 km s^{-1}, and hence also hosts an AGN (Sajina et al. 2008). The presence of a broad-line argues against this source being Compton-thick. There are cases of course of broad-line QSOs associated with Compton-thick AGN but these cases are rare (Braito et al. 2004).

4. Discussion

4.1. The efficiency of the high-τ method for finding Compton-thick AGN

Silicate absorption features in a few (U)LIRGS in the local Universe known to be associated with Compton-thick AGN (e.g. NGC 6240; Armus et al. 2006), prompts us to investigate whether a high optical depth at 9.7 μm could provide a reliable diagnostic for the presence of these nuclei. We can reliably identify Compton-thick AGN in the nearby Universe by means of X-ray spectroscopy, owing to their high X-ray brightness. We argue that six out of nine highly absorbed sources at 9.7 μm ($\tau_{9.7} > 1$), in the 12 μm IRAS Seyfert sample, with X-ray spectra available in the literature are probably associated with Compton-thick nuclei. In any case, all nine sources are heavily obscured AGN.

Since these are nearby AGN ($z < 0.06$), they should contribute only a small fraction to the X-ray background. The peak of the X-ray background is produced at $z \sim 0.7-1$ from objects with intrinsic luminosities around the "knee" of the luminosity function, i.e., $\sim 10^{43}-10^{44}$ erg s^{-1} (Gilli et al. 2007). The median X-ray luminosity (uncorrected for absorption) of our six local Compton-thick AGN is $\sim 0.5 \times 10^{42}$ erg s^{-1}. Assuming a correction of about 33 for the intrinsic X-ray luminosity (Comastri 2004), this translates to $\approx 2 \times 10^{43}$ erg s^{-1}. Hence, AGN with comparable luminosity, but at higher redshift, are the typical AGN responsible for the peak of the X-ray background.

At higher redshift, the fraction of candidate Compton-thick AGN is more uncertain. This fraction can be derived indirectly from the X-ray to IR luminosity ratio. If we take only the X-ray detections into account, this is close to 66%. When we also consider the upper limits, we find that the uncertainty becomes large: the fraction of Compton-thick sources could vary between 33% and 83%.

The frequency of Compton-thick AGN measured above is comparable to or higher than derived by other mid-IR methods for finding Compton-thick sources. For example, on the basis of X-ray stacking analyses, several authors (e.g. Daddi et al. 2007; Fiore et al. 2008; Georgantopoulos et al. 2008) proposed that the 24 μm-excess sources are good candidates for hosting Compton-thick nuclei. However, because of the lack of X-ray spectroscopy the fraction of Compton-thick sources cannot be readily quantified. Based on brighter sources with X-ray spectroscopy in the GOODS (Georgantopoulos et al. 2011), AEGIS (Georgakakis et al. 2010) and SWIRE fields (Lanzuisi et al. 2009), the fractions of Compton-thick sources found among IR-excess AGN range between 0% and 50%. Another widely applied mid-IR method for the selection of Compton-thick AGN (Alexander et al. 2008) relies on low X-ray to IR ratios. The principle behind this method is that a low L_X/L_{IR} ratio is a sign of heavy obscuration (but see Yaqoob & Murphy 2011; Georgakakis et al. 2010).

Although we have shown that the success rate of our technique in finding Compton-thick AGN is close to 70%, at least among optically confirmed Seyferts in the local Universe, there are two caveats. First, the detection of this feature alone does not imply the presence of an AGN in these systems. There are star-forming systems with large absorption features at 9.7 μm that are associated instead with star-forming galaxies. One case is NGC 3628 for which $\tau_{9.8} = 1.64$ (Brandl et al. 2006), although the X-ray emission in this system does not come from an AGN (Dahlem et al. 1996). In other words, the high $\tau_{9.7}$ optical depth characterises systems with large amounts of dust but does not necessarily prove the presence of an AGN. The second caveat has to do with the completeness of our method. There are well-known Compton-thick sources in the literature that contain no significant 9.7 μm absorption. We discuss this in detail in the following section.

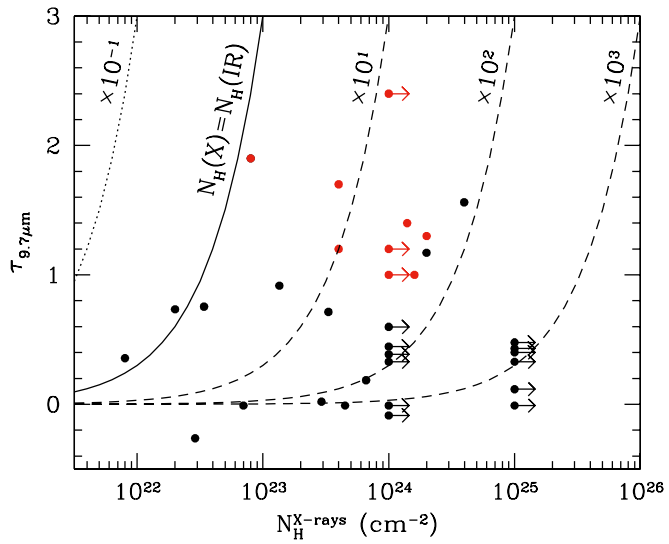

Fig. 4. Optical depth at 9.7 μm versus X-ray hydrogen column density for the Shi et al. (2006) sample (black points) and the optically-thick AGN in the IRAS sample of Wu et al. (2009) (red points). The solid line marks the region where the X-ray N_H equals that inferred from $\tau_{9.7}$, assuming a Milky-Way extinction curve.

4.2. Si optical depth versus X-ray column density

Shi et al. (2006) described observations of 9.7 μm features in 97 AGN including a wide range of types. They found that the strength of the silicate feature correlates with the hydrogen column density, derived from X-ray observations in the sense that the low column densities correspond to silicate emission, while high columns correspond to silicate absorption. They point out that the column densities derived from X-ray spectral fitting are always higher than those estimated on the basis of the Si optical depths. Moreover, there appears to be a large scatter between the X-ray and the 9.7 μm column density in the sense that the same $\tau_{9.7}$ corresponds to X-ray column densities that could differ by as much as an order of magnitude. This result can be seen more clearly in Fig. 4, where we plot the 9.7 μm optical depth as a function of the X-ray column density for both the 12 μm sample as well as the sample of Shi et al. (2006). We note that the latter is based mainly on the optically selected sample of Risaliti et al. (1999). Some column densities in this sample were revised by Malizia et al. (2009) and we include these updated values in Fig. 4. This figure clearly shows that the majority of the optically thick sources detected in the mid-IR display Compton-thick absorption at X-ray wavelengths. In addition we see that there are numerous Compton-thick AGN according to X-ray spectroscopy that have optical depths $\tau_{9.7} < 1$.

Perhaps the most well studied case of a low Si τ Compton-thick source is NGC 1068. The X-ray column density of this

Seyfert-2 galaxy is $N_{\rm H} > 10^{25}$ cm^{-2} as derived from high energy X-ray spectroscopy (Matt et al. 2004) with the *BeppoSAX* mission. However, the mid-IR spectrum shows no prominent 9.7 μm absorption (Sturm et al. 2000). In Shi et al. (2006) there are many more examples of Compton-thick nuclei which are optically thin at 9.7 μm (see Fig. 4). From the above discussion, it becomes clear that although the presence of a high-τ absorption feature implies the presence of a Compton-thick AGN, with a probability of roughly 70%, the opposite is not true, i.e., there are many Compton-thick AGN which are not significantly absorbed at 9.7 μm.

The reason for this could be that the X-ray and infrared emitting regions are not physically coincident and the infrared arises from a region further away from the accretion disk. It is possible that within the framework of a clumpy torus model (see e.g. Nenkova et al. 2008; Wada et al. 2009; Nikutta et al. 2009), the X-ray emission from the AGN could be obscured by a circumnuclear cloud, while the infrared emission, which is produced at larger distances from the AGN, could experience low or no obscuration at all (see Fig. 5 in Shi et al. 2006). Spoon et al. (2007) proposed that the depth of the Si 9.7 μm feature can be used as a tool to predict the obscuring dust distribution. In this scenario, high silicate depths correspond to sources embedded in a smooth dust distribution, while low depths correspond to those covered by patchy absorbers.

4.2.1. Comparison with previous results

We compare our results with the work of Alexander et al. (2008), who searched for Compton-thick AGN in the CDF-N using both IRS spectroscopy in combination with the $L_{\rm X}/L_{6\ \mu{\rm m}}$ ratio. Alexander et al. (2008) discussed the properties of two sources with available mid-IR IRS spectroscopy in the CDF-N, claiming that both could be associated with Compton-thick AGN. One (HDF-oMD49) is an optically identified AGN that is formally undetected in the 2 Ms data Alexander et al. (2003). The *Spitzer* IRS spectrum and spectral energy distribution of this object is AGN dominated. On the basis of the source's low $L_{\rm X}/L_{\rm IR}$ ratio, Alexander et al. (2008) argue that this AGN is Compton-thick. The other source (SMMJ123600+621047) is a $z = 2.002$ submillimeter-emitting galaxy (SMG) with a mid-IR-bright AGN (Pope et al. 2008) that is again undetected in the 2 Ms CDF-N data. The $L_{\rm X}/L_{6\ \mu{\rm m}}$ luminosity ratio indicates that it hosts a Compton-thick AGN, although optical and near-IR spectroscopic observations do not reveal the signatures of AGN activity, leaving open the possibility that this source is associated with a star-forming galaxy and not with an AGN. None of these sources display a $\tau > 1$ 9.7 μm absorption feature in their IRS spectrum.

5. Summary

The goal of this work has been to investigate whether the presence of high-absorption at mid-IR wavelengths ($\tau_{9.7} > 1$) can be used as an efficient means for identifying highly obscured or even Compton-thick AGN. Our conclusions can be summarised as follows:

- Our re-analysis of *Spitzer*-IRS spectra shows that there are eleven AGN with $\tau_{9.7\ \mu{\rm m}} > 1$ in the 12 μm Seyfert IRAS sample. For nine sources X-ray spectroscopic observations are available in the literature. The X-ray spectra show that a large fraction (six of nine) is probably associated with Compton-thick AGN. The success rate of this method is comparable to or even higher than those of other methods using either mid-IR photometric information or the X-ray to IR luminosity ratio.
- Even though optical thickness in the MIR, as determined by 9.7 micron Si absorption with $\tau > 1$ can be efficiently used to identify Compton-thick sources in the local Universe with a high success rate, this method cannot provide complete samples of these sources. This is because a large fraction of Compton-thick sources do not have large high Si optical depths. This could possibly be explained within the framework of a clumpy torus model.
- Using *Spitzer*-IRS spectra in the CDF and the FLS surveys, we have compiled a sample of 12 sources in total, with $\tau_{9.7} > 1$ at higher redshift ($z = 0.87-2.70$). These are selected to have weak PAH features to maximise the probability that they host an AGN. The vast majority of sources in the CDFs (six out of seven) are detected in the X-rays, while all five FLS sources remain undetected. For the X-ray detections, the high X-ray luminosities ($>2\times10^{42}$ erg s^{-1}) confirm that all these sources are AGN. For two FLS sources, their optical line emission also indicates that an AGN is present. Because our sources are faint in X-rays, we are unable to ascertain from X-ray spectroscopy whether at least some of our sources are Compton-thick. The use of the $L_{\rm X}/L_{6\ \mu{\rm m}}$ ratio indicates that the success rate of the high-τ method in identifying Compton-thick AGN could be about 66% (4/6), if we consider X-ray detections only. However, it can be as low as ~33% (4/12), or as high as 83% under the extreme assumptions that all the X-ray upper limits are either associated or not associated with Compton-thick sources. Deeper X-ray spectroscopy will be needed to properly constrain the exact fraction of Compton-thick AGN among high-z, high-τ sources.

In the future, observations with the JWST will be able to identify numerous galaxies with deep Si features that could be used to compile large candidate Compton-thick AGN samples.

Acknowledgements. I.G. and A.C. acknowledge support by the European Community through the Marie Curie fellowship FP7-PEOPLE-IEF-2008 Prop. 235285 under the Seventh Framework Programme (FP7/2007-2013). K.D. also acknowledges support by the European Community through a Marie Curie Fellowship (PIEF-GA-2009-235038) awarded under the Seventh Framework Programme (FP7/2007-2013) The *Chandra* data were taken from the *Chandra* Data Archive at the *Chandra* X-ray Center. This work is based on observations made with the *Spitzer* Space Telescope, which is operated by the Jet Propulsion Laboratory, California Institute of Technology under contract with NASA.

References

Ajello, M., Rau, A., Greiner, J., et al. 2008, ApJ, 673, 96
Akylas, A., & Georgantopoulos, I. 2009, A&A, 500, 999
Akylas, A., Georgantopoulos, I., Georgakakis, A., Kitsionas, S., & Hatziminaoglou, E. 2006, A&A, 459, 693
Alexander, D. M., Bauer, F. E., Brandt, W. N., et al. 2003, AJ, 126, 539
Alexander, D. M., Chary, R. R., Pope, A., et al. 2008, ApJ, 687, 835
Armus, L., Bernard-Salas, J., Spoon, H. W. W., et al. 2006, ApJ, 640, 204
Armus, L., Charmandaris, V., Bernard-Salas, J., et al. 2007, ApJ, 656, 148
Arnaud, K. A. 1996, in Astronomical Data Analysis Software and Systems V, ed. Jacoby, G., & Barnes, J., ASP Conf. Ser., 101, 17
Barger, A. J., Cowie, L. L., & Wang, W.-H. 2008, ApJ, 689, 687
Bauer, F. E., Alexander, D. M., Brandt, W. N., et al. 2004, AJ, 128, 2048
Bauer, F. E., Yan , L., Sajina, A., & Alexander, D. M. 2010, ApJ, 710, 212
Bianchi, S., Piconcelli, E., Chiaberge, M., et al. 2009, A&A, 695, 781
Braito, V., Franceschini, A., Della Ceca, R., et al. 2003, A&A, 398, 107
Braito, V., Della Ceca, R., Piconcelli, E., et al. 2004, A&A, 420, 79
Brightman, M., & Nandra, K. 2011, MNRAS, 413, 1206
Brandl, B. R., Bernard-Salas, J., Spoon, H. W. W., et al. 2006, ApJ, 653, 1129
Brandt, W. N., & Hasinger, G. 2005, ARA&A, 43, 827

Brassington, N. J., Ponman, T. J., & Read, A. M. 2007, MNRAS, 377, 1439
Burlon, D., Ajello, M., Greiner, J., et al. 2011, Apj, 728, 58
Cash, W. 1979, ApJ, 228, 939
Chapman, S. C., Blain, A. W. Smail, I., & Ivison, R. J. 2005, ApJ, 622, 772
Chary, R., & Elbaz, D. 2001, ApJ, 556, 562
Churazov, E., Sunyaev, R., Revnivtsev, M., et al. 2007, A&A, 467, 529
Clements, D. L., McDowell, J. C., Shaked, S., et al. 2002, ApJ, 581, 974
Comastri, A. 2004, ASSL, 308, 245
Comastri, A., Ranalli, P., Iwasawa, K., et al. 2011, A&A, 526, L9
Cusumano, G., La Parola, V., Segreto, A., et al. 2010, A&A, 510, A48
Daddi, E., Alexander, D. M., Dickinson, M., et al. 2007, ApJ, 670, 173
Dadina, M. 2008, A&A, 485, 417
Dahlem, M., Heckman, T. M., Fabbiano, G., Lehnert, M. D., & Gilmore, D. 1996, ApJ, 461, 724
Damen, M., Labbe, I., van Dokkum, P. G., et al. 2011, ApJ, 727, 1
Dasyra, K. M., Yan, L., Helou, G., et al. 2009, ApJ, 701, 1123
Donley, J. L., Rieke, G. H., Alexander, D. M., Egami, E., & Pérez-González, P. G. 2010, ApJ, 719, 1393
Eckart, M. E., McGreer, I. D., Stern, D., Harrison, F. A., & Helfand, D. J. 2010, ApJ, 708, 584
Egami, E., Neugebauer, G., & Soifer, B. T. 2006, AJ, 131, 1253
Feruglio, C., Daddi, E., Fiore, F., et al. 2011, ApJ, 729, L4
Fiore, F., Grazian, A., Santini, P., et al. 2008, ApJ, 672, 94
Fiore, F., Puccetti, S., Brusa, M., et al. 2009, ApJ, 693, 447
Franceschini, A., Braito, V., Persic, M., et al. 2003, MNRAS, 343, 1181
Frontera, F., Orlandini, M., & Landi, R. 2007, ApJ, 666, 86
Genzel, R., Lutz, D., Sturm, E., et al. 1998, ApJ, 498, 579
Georgakakis, A., Rowan-Robinson, M., Babbedge, T. S. R., & Georgantopoulos, I. 2007, MNRAS, 377, 203
Georgakakis, A., Rowan-Robinson, M., Nandra, K., et al. 2010, MNRAS, 406, 420
Georgantopoulos, I., Georgakakis, A., Rowan-Robinson, M., & Rovilos, E. 2008, A&A, 484, 671
Georgantopoulos, I., Akylas, A., Georgakakis, A., & Rowan-Robinson, M. 2009, A&A, 507, 747
Georgantopoulos, I., Rovilos, E., Akylas, A., & Xilouris, E. 2010, A&A, 520, L4
Georgantopoulos, I., Rovilos, E., & Comastri, A. 2011, A&A, 526, A86
Gilli, R., Comastri, A., & Hasinger, G. 2007, A&A, 463, 79
González-Martin, O., Masegosa, J., Márquez, I., Guainazzi, M., & Jiménez-Bailón, E. 2009, A&A, 506, 1107
Goulding, A., Alexander, D., Mullaney, J., et al. 2011, MNRAS, 411, 1231
Guainazzi, M., Matt, G., & Perola, G. C. 2005, A&A, 444, 119
Helou, G., Soifer, B. T., & Rowan-Robinson, M. 1985, ApJ, 298, L7
Hernán-Caballero, A., Pérez-Fournon, Hatziminaoglou, E., et al. 2009, MNRAS, 395, 1695
Imanishi, M., Terashima, Y., Anabuki, N., & Nakagawa, T. 2003, ApJ, 596, 167
Imanishi, M., Maiolino, R., & Nakagawa, T. 2010, ApJ, 709, 801
Iwasawa, K., Sanders, D. B., Evans, A. S., et al. 2005, MNRAS, 357, 565
Iwasawa, K., Sanders, D. B., Evans, A. S., et al. 2009, ApJ, 695, L103
Iwasawa, K., Mazzarella, J. M., Surace, J. A., et al. 2011, A&A, 528, A137
Lanzuisi, G., Piconcelli, E., Fiore, F., et al. 2009, ApJ, 498, 67
Luo, B., Bauer, F. E., Brandt, W. N., et al. 2008, ApJS, 179, 19
Lutz, D., Maiolino, R., Spoon, H. W. W., & Moorwood, A. F. M. 2004, A&A, 418, 465
Magnelli, B., Elbaz, D., Chary, R. R., et al. 2009, A&A, 496, 57
Maiolino, R., Shemmer, O., Imanishi, M., et al. 2007, A&A, 468, 979
Malizia, A., Stephen, J. B., Bassani, L., et al. 2009, MNRAS, 399, 944
Marconi, A., Risaliti, G., Gilli, R., et al. 2004, MNRAS, 351, 169
Martínez-Sansigre, A., Rawlings, S., Lacy, M., et al. 2005, Nature, 436, 666
Matt, G., Bianchi, S., Guainazzi, M., & Molendi, S. 2004, A&A, 414, 155
Merloni, A., & Heinz, S. 2008, MNRAS, 388, 1011
Moran, E. C., Lehnert, M. D., & Helfand, D. J. 1999, ApJ, 526, 649
Moretti, A., Pagani, C., Cusumano, G., et al. 2009, A&A, 493, 501
Murphy, K. D., & Yaqoob, T. 2009, MNRAS, 397, 1549
Murphy, E. J., Chary, R.-R., Alexander, D. M., et al. 2009, ApJ, 698, 1380
Nenkova, M., Sirocky, M. M., Ivezic, Z., & Elitzur, M. 2008, ApJ, 685, 147
Netzer, H., Lutz, D., Schweitzer, M., et al. 2007, ApJ, 666, 806
Nikutta, R., Elitzur, M., & Lacy, M. 2009, ApJ, 707, 1550
Paltani, S., Walter, R., McHardy, I. M., et al. 2008, A&A, 485, 707
Polletta, M., Tajer, M., Maraschi, L., et al. 2007, ApJ, 663, 81
Pope, A., Borys, C., Scott, D., et al. 2005, MNRAS, 358, 149
Pope, A., Chary, R.-R., Alexander, D. M., et al. 2008, ApJ, 675, 1171
Ptak, A., Heckman, T., Levenson, N. A., Weaver, K., & Strickland, D. 2003, ApJ, 592, 782
Ptak, A., Mobasher, B., Hornschemeier, A., Bauer, F., & Norman, C. 2007, ApJ, 667, 826
Richards, G. T., Lacy, M., & Storrie-Lombardi, L. J. 2006, ApJS, 166, 470
Risaliti, G., Maiolino, R., & Salvati, M. 1999, ApJ, 522, 157
Rosenthal, D., Bertoldi, F., & Drapatz, S. 2000, A&A, 356, 705
Rush, B., Malkan, M. A., & Spinoglio, L. 1993, ApJS, 89, 1
Sajina, A., Yan, L., Armus, L., et al. 2007, ApJ, 664, 713
Sajina, A., Yan, L., Lutz, D., et al. 2008, ApJ, 683, 659
Sazonov, S., Krivonos, R., Revnivtsev, M., Churazov, E., & Sunyaev, R. 2008, A&A, 482, 517
Shi, Y., Rieke, G. H., Hines, D. C., et al. 2006, ApJ, 653, 127
Silva, L., Maiolino, R., Granato, G. L. 2004, MNRAS, 355, 973
Smith, J. D. T., Draine, B. T., Dale, D. A., et al. 2007, ApJ, 656, 770
Soifer, B. T., Neugebauer, G., Matthews, K., Egami, E., & Weinberger, A. J. 2002, AJ, 124, 2980
Soltan, A. 1982, MNRAS, 200, 115
Spoon, H. W. W., Marshall, J. A., Houck, J. R., et al. 2007, ApJ, 654, L49
Sturm, E., Lutz, D., Tran, D., et al. 2000, A&A, 358, 481
Tozzi, P., Gilli, R., Mainieri, V., et al. 2006, A&A, 451, 457
Treister, E., Urry, C. M., & Virani, S. 2009a, ApJ, 696, 110
Treister, E., Cardamone, C. N., Schawinski, K., et al. 2009b, ApJ, 706, 535
Tueller, J., Mushotzky, R. F., Barthelmy, S., et al. 2008, ApJ, 681, 113
Tzanavaris, P., Georgantopoulos, I., & Georgakakis, A. 2006, A&A, 454, 447
Vignati, P., Molendi, S., Matt, G., et al. 1999, A&A, 349, L57
Wada, K., Papadopoulos, P. P., & Spaans, M. 2009, ApJ, 702, 63
Winter, L. M., Mushotzky, R. F., Reynolds, C. S., & Tueller, J. 2009, ApJ, 690, 1322
Wu, Y., Charmandaris, V., Huang, J., Spinoglio, L., & Tommasin, S. 2009, ApJ, 701, 658
Yan, L., Sajina, A., Fadda, D., et al. 2007, ApJ, 658, 778
Yaqoob, T., & Murphy, K. 2011, MNRAS, 412, 835
Zakamska, N. 2010, Nature, 465, 60
Zakamska, N. L., Strauss, M. A., Krolik, J., et al. 2003, AJ, 126, 2125